Vibrational vs. translational energy in promoting a prototype metal–hydrocarbon insertion reaction

David L. Proctor and H. Floyd Davis*

Department of Chemistry and Chemical Biology, Baker Laboratory, Cornell University, Ithaca, NY 14853-1301

Edited by F. Fleming Crim, University of Wisconsin, Madison, WI, and approved April 17, 2008 (received for review February 5, 2008)

The reaction Y + CH_4 → $HYCH_3$ → YCH_2 + H_2 is initiated by C–H insertion involving a 20 ± 3 kcal/mol potential energy barrier. The reaction is studied in crossed molecular beams under two different conditions with nearly the same total energy. One experiment is carried out at a collision energy of 15.1 kcal/mol with one quantum of CH_4 antisymmetric (ν_3) stretching vibrational excitation (8.63 kcal/mol), the other at a collision energy of 23.8 kcal/mol. The reaction cross-section for C–H stretch excited methane (σ_s) is found to be at least a factor of 2.2 times larger than for ground-state methane (σ_g) at the same total energy.

mode-specific chemistry | potential energy barrier | reaction dynamics

The concepts of early and late potential energy barriers made it possible to rationalize in simple, intuitive terms the roles of reactant translational and vibrational energy in promoting atom + diatom reactions (1). The observation of mode- and bond-specific effects in gas phase reactions such as Cl + CH_4 → HCl + CH_3 and Cl + H_2O → HCl + OH have illustrated that the dynamics of polyatomic systems involving multiple vibrational degrees of freedom can also be highly sensitive to the reactant vibrational state (2, 3).

In a recent study, Yan and coworkers provided the first direct comparison of C–H reactant vibrational energy to reactant translational energy in promoting the Cl + CHD_3 → HCl + CD_3 abstraction reaction (4). Although C–H antisymmetric vibrational excitation enhanced reactivity, it was found to be somewhat *less* effective than an equivalent amount of reactant translational energy. However, CHD_3 bending excitation induced by thermal excitation was somewhat *more* effective in promoting reaction than an equivalent amount of translational energy. For gaseous polyatomic systems, different forms of reactant energy may not be equivalent in facilitating passage through the transition state for atom transfer (2–5).

The dissociative adsorption of methane (CH_4) on a metal surface is the rate-limiting step in the steam re-forming of methane, used to produce ≈9 million tons of hydrogen annually in the United States. It is well established that reactant translational *and* vibrational excitation are both effective in promoting this activated process (6). Significant mode- and bond-specific effects have been observed for this class of reaction. Smith and coworkers showed that antisymmetric CH_4 vibrational excitation (ν_3) is somewhat more effective than an equivalent amount of translational energy in promoting reaction on a Ni(111) surface (7), in contrast to earlier work on Ni(100) (6) and Pt(111) (8), where translational energy was more effective in promoting reaction. Juurlink *et al.* (9) demonstrated that CH_4 overtone bending excitation ($3\nu_4$) is much less effective than ν_3 on Ni(100) and Ni(111), despite the higher energy of $3\nu_4$. Maroni and coworkers (10) found that CH_4 symmetric excitation (ν_1) is about an order of magnitude more effective than antisymmetric stretching (ν_3) in promoting reaction on Ni(100) at nearly identical total energies. The latter result is particularly striking because it demonstrates that, even for a complex polyatomic reaction at the gas–solid interface, two reactant vibrational states that differ only in the relative phases of atomic motions can have profoundly different reactivities.

The activation of hydrocarbon C–H bonds by transition metal complexes is a topic of considerable current interest (11, 12). Insight into the factors controlling the kinetics and thermodynamics of these processes has been derived through electronic structure theory (13). Unfortunately, the presence of multiple ligands in transition metal complexes makes theoretical calculations difficult. Consequently, substantial effort has been devoted to carrying out calculations on model systems involving insertion of isolated transition metal *atoms* into C–H and C–C bonds (14, 15). Interestingly, recent theoretical work on the dynamics of the dissociative adsorption of methane on Ir(111) (16) and Ni(111) (17) surfaces indicate that the metal lattice undergoes reconstruction during reaction, with a local surface metal atom undergoing significant (0.6 Å) displacement outward from the surface. Understanding the reactivity of isolated transition metal atoms with methane may thus provide insight into the dissociative adsorption process.

Early second-row transition metal atoms have few valence electrons (e.g., $5s^24d^1$ for Y), yet form strong M–H and M–C bonds (14, 15). However, neutral metal atoms encounter substantial potential energy barriers for insertion into C–H bonds of saturated hydrocarbon molecules (14, 15). One of the simplest prototypical neutral bimolecular reactions involving a transition metal center with methane is Y + CH_4 → $HYCH_3$ → YCH_2 + H_2 (Fig. 1). This reaction involves initial insertion of the metal center into a C–H bond of methane by passage over a potential energy barrier calculated by Wittborn and coworkers (14) to lie 20.5 kcal/mol above the reactants. For the analogous reaction involving ethane (C_2H_6), the potential energy barrier for C–H insertion was measured to be 19.9 ± 3.0 kcal/mol (18). As expected, collisions at translational energies below the barrier were unreactive, but formation of both YC_2H_4 + H_2 and YH_2 + C_2H_4 was observed at collision energies above the barrier (18). For Y + CH_4, the initial insertion step can be viewed as involving elongation of a C–H bond in the CH_4 reactant (Fig. 1) with simultaneous formation of two new bonds producing $HYCH_3$. By analogy with the surface experiments, and because C–H stretching is likely to be an important component of the reaction coordinate, C–H vibrational excitation might be effective in promoting insertion. However, the antisymmetric CH_4 stretching mode (ν_3) is a normal mode involving motion of all four atoms in methane, whereas insertion involves a local interaction with a single C–H bond. To date there has been no systematic study in which translational energy is compared with vibrational energy in promoting an insertion reaction.

Results

We conducted crossed molecular beam reactive scattering experiments between Y atoms and ground-state CH_4 at beam

Author contributions: D.L.P. and H.F.D. designed research, performed research, analyzed data, and wrote the paper.

The authors declare no conflict of interest.

This article is a PNAS Direct Submission.

*To whom correspondence should be addressed. E-mail: hfd1@cornell.edu.

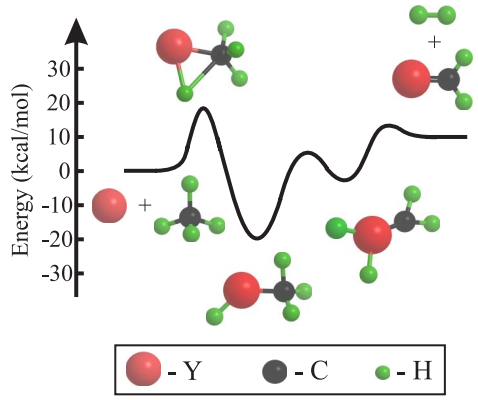

Fig. 1. Schematic energy level diagram for Y + $CH_4 \rightarrow YCH_2 + H_2$ reaction.

velocities providing 23.8 ± 1.5 kcal/mol translational energy and between Y and CH_4 ($\nu_3 = 1$) at beam velocities providing 15.1 ± 0.9 kcal/mol of translational energy. Fig. 2 shows the total reactant energy distributions for the two sets of experiments. The vibrational energy in the second experiment, provided by absorption of a 3,018 cm^{-1} photon produced by an infrared optical parametric oscillator (OPO), makes the total energy essentially identical in each experiment. Mass-selected time-of-flight (TOF) distributions of YCH_2 reaction products were recorded at several laboratory angles relative to the beams for both experiments. Calculated TOF distributions based on iteratively adjusted center-of-mass (CM) frame product translational energy and angular distributions were fit to the data by using forward convolution over known beam velocity distributions and instrument functions.

Fig. 3 shows the laboratory angular distribution of YCH_2 products at the 23.8 kcal/mol collision energy, as well as the CM translational energy distribution used in the fit. The CM angular distribution, $T(\theta)$, was isotropic as anticipated for a reaction involving complexes with lifetimes longer than their rotational periods. Fig. 4 shows the TOF distributions for the YCH_2 products. At this collision energy (i.e., above the barrier), reaction of ground-state CH_4 leads to formation of $YCH_2 + H_2$, with the product translational energy $P(E)$ peaking near 3 kcal/mol and extending to 11 kcal/mol, with $\langle P(E) \rangle$ = 3.6 kcal/mol. The TOFs and lab angular distribution for the 15.1 kcal/mol collision energy with vibrational excitation were fit by using the same $P(E)$ and CM angular distribution and appear similar.

We have found that the reaction cross-section rises sharply with reactant collision energy. The dependence of the reactive signal on collision energy places the potential energy barrier for reaction at 20 ± 3 kcal/mol. The uncertainty in this value results

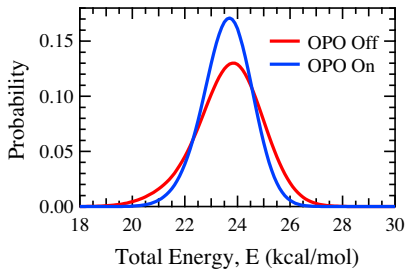

Fig. 2. Probability distribution function for total reactant energy in ''OPO Off'' and ''OPO On'' experiments. In OPO Off experiments, all reactant energy is translational; in OPO On experiments, total reactant energy includes 8.63 kcal/mol of vibrational excitation in the CH_4 antisymmetric stretch (ν_3) vibrational mode.

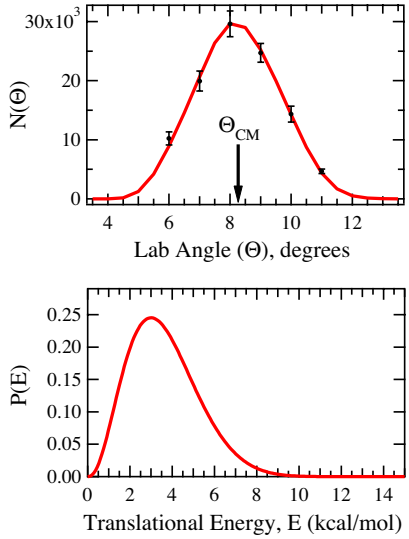

Fig. 3. Laboratory angular distribution with marked center-of-mass scattering angle and product translational energy release distribution, $P(E)$ for Y + $CH_4 \rightarrow YCH_2 + H_2$ at E_{coll} = 23.8 kcal/mol with OPO Off. Data in black, fit in red, and error bars are 90% confidence intervals.

primarily from the spread in collision energies for each experiment and from the presence of spin orbit excited $Y(^2D_{1/2})$, which lies 1.5 kcal/mol above the ground $Y(^2D_{3/2})$ state, in the atomic beam. The product translational energy release data place the $YCH_2 + H_2$ product asymptote ≈11 kcal/mol above the reactants. This is consistent with product energetics calculated by using the results of recent theoretical work that places this value near 12 kcal/mol (19). The rate-limiting step in the reaction thus corresponds to passage of the system over the initial barrier for C–H insertion.

At a nominal mean collision energy of 18.6 kcal/mol, weak product signal was observed for ground-state CH_4 molecules. At a collision energy of 15.1 kcal/mol, no reaction was observed without OPO irradiation. Inelastic scattering experiments indicated that, at this collision energy, the nonreactively scattered Y atoms are strongly forward-scattered in the CM frame, indicating the occurrence of direct inelastic scattering without appreciable formation of long-lived YCH_4 complexes. The absence of complex formation at collision energies below the barrier is anticipated because neutral metal–alkane σ-complexes are bound by no more than 1–2 kcal/mol (20). At this collision energy, which is well below the C–H insertion barrier for ground vibrational state CH_4 molecules, a strong YCH_2 signal is observed when the CH_4 molecules are optically pumped to the C–H antisymmetric stretching level (ν_3) just before collision. The observed YCH_2 signal level as a function of OPO pulse energy (Fig. 5) indicates that the transition is easily saturated because of the narrow bandwidth of the OPO. Thus, C–H vibrational excitation opens up reactions of colliding pairs at collision energies that were completely unreactive for unexcited methane.

To obtain quantitative insight into the relative efficacy of *vibrational vs. translational* energy in promoting insertion, we measured the ratio of total reaction cross-sections for stretch excited methane (σ_s) to that for ground-state methane (σ_g) accelerated to the same total energy. For each experiment σ can be calculated as the total signal level in the center-of-mass frame divided by the product of the number density of each reactant in the interaction volume and the relative velocity of the reactants (21). Because our target is a ratio of cross-sections, we use ratios of these parameters rather than absolute values. In this calculation we made each assumption or approximation conserva-

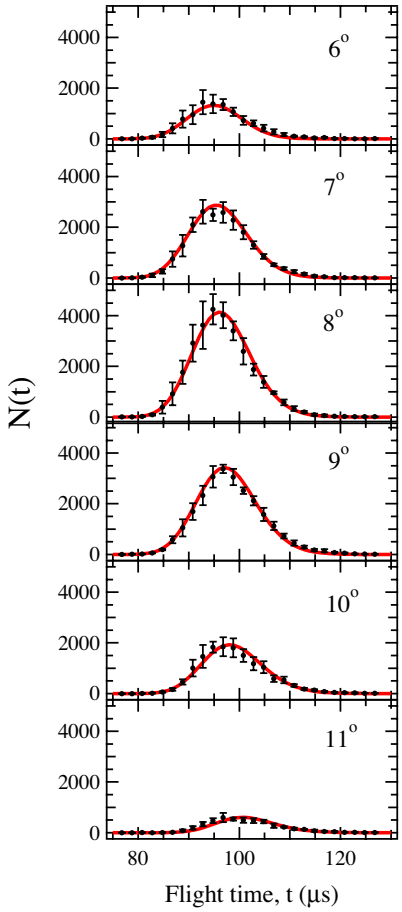

Fig. 4. Laboratory time-of-flight distributions for YCH_2 products at indicated laboratory angles with OPO Off. Filled circles denote experimental data and solid line is calculated distribution using $P(E)$ from Fig. 2 and isotropic center-of-mass angular distribution $T(\theta)$. Data in black, fit in red, and error bars are 90% confidence intervals.

tively, that is, in the direction that always produces a *strict lower limit* to the reactivity ratio (σ_s/σ_g). The ratio of center-of-mass signal levels was calculated during forward convolution fitting of the data. The ratio of Y beam number densities was measured by pulsed laser-induced fluorescence on the $^2P_{1/2} \leftarrow {}^2D_{3/2}$ line at 359.4 nm directly in the interaction region. The ratio of CH_4 number densities was taken to be the ratio of the CH_4 fractions in the gas mixtures. In the optical pumping experiment, the effective CH_4 ($\nu_3 = 1$) number density is also proportional to the fraction of molecules pumped. This fraction is the product of

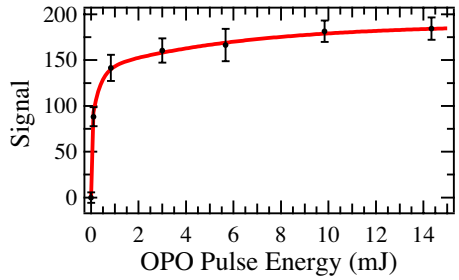

Fig. 5. Saturation curve showing YCH_2 signal level recorded at laboratory center-of-mass angle as a function of OPO pulse energy. Data in black, fit in red, and error bars are 90% confidence intervals.

three factors: the fractional population of the lower state of the optical transition before interaction with the OPO, the fraction of this population excited by the OPO, and the fraction of the gas pulse illuminated by the OPO beam. Taking these factors into account (as described in *Experimental Methods*), we calculate that the total reactive cross-section of the CH_4 antisymmetric stretch is $\geq$2.2 times the cross-section for ground-state CH_4.

Discussion

Our measured value of $\sigma_s/\sigma_g \geq 2.2$ represents a strict lower limit to the ratio of the total reaction cross-section for $Y + CH_4 \rightarrow YCH_2 + H_2$ at $E_{coll} = 15.1$ kcal/mol with one quantum of C–H antisymmetric stretching excitation (σ_s) to that at $E_{coll} = 23.8$ kcal/mol with no OPO irradiation (σ_g). In the OPO-off case, it is important to consider the role of vibrationally excited CH_4 molecules that may be present because of thermal excitation. It is known that vibrational energy is only cooled efficiently within vibrational levels of similar energies on supersonic expansion (22). By using the CH_4 vibrational frequencies and degeneracies, at 300 K $\approx$0.70% of the CH_4 molecules are vibrationally excited, with all but a negligible fraction in the low-energy excited bending levels ν_4 (1,306 cm^{-1}) and ν_2 (1,534 cm^{-1}). In experiments at 15.1 kcal/mol, it is unlikely that molecules containing vibrational energy because of thermal excitation (but are not pumped by the OPO) contribute significantly to the observed reactive signal. However, in the experiments at $E_{coll} = 23.8$ kcal/mol, a significant fraction of the observed signal could in principle result from reactions of bend-excited CH_4. To explore this possibility, experiments were carried out at the same collision energy by using a nozzle heated to 380 K, where the population of bend-excited methane should be $\approx$4 times that at 300 K. No evidence for enhanced reactivity attributable to bend-excited methane was observed, strongly suggesting that the OPO off-signal is not dominated by reaction of bend-excited methane.

In reactions involving elimination of H or H_2, angular momentum conservation can play an important role in the dynamics. In particular, if complexes are produced with large total angular momenta, because of the small reduced mass of the products, centrifugal barriers in the exit channel can increase the fraction of complexes decomposing to reactants rather than to products (23). The present experiments were carried out by pumping the ν_3 Q(1) line of a jet-cooled sample of CH_4 molecules. In the reaction of vibrationally excited molecules, only one quantum of rotational angular momentum ($J = 1$) contributes to the total angular momentum of the $HYCH_3$ complexes. In reactions at high collision energy, although all J levels can contribute, because rotational cooling is expected to be nearly complete ($T < 5$ K), the contribution from higher rotational levels of methane will be negligible. Because of the large potential energy barrier to reaction, in particular, for ground vibrational level molecules, reactions from small impact parameter (b) collisions will be dominant. Consequently, the maximum total angular momentum of the complexes, which is primarily determined by the orbital angular momentum $L = \mu v b$, is highly restricted in both experiments. Therefore, the fraction of insertion complexes decaying to products should not differ significantly between the two experiments. Indeed, in studies of nonreactively scattered Y atoms at wide laboratory angles (corresponding to CM angles near 180°) we were unable to observe any statistically significant difference in nonreactive scattering of Y atoms with the OPO on and off. Because of this, and because the barrier to insertion is the largest barrier on the PES, most $HYCH_3$ complexes decay to $YCH_2 + H_2$ rather than back to reactants.

The potential energy barriers for insertion of ground-state neutral transition metal atoms (having n valence electrons) into C–H bonds of hydrocarbon molecules result from the repulsive

interactions between the ground-state $d^{n-2}s^2$ or high-spin $d^{n-1}s^1$ electronic configurations of most neutral metal atoms and the directional sp^3 hybridized C–H σ-bond (15, 20). Successful reaction requires access to the low-spin $d^{n-1}s^1$ or d^ns^0 electronic configurations able to minimize long-range repulsive interactions and form the two new covalent bonds in the insertion complex. In the case of Y + CH_4, the adiabatic barrier for insertion results from the avoided crossings of diabatic curves associated with the repulsive doublet ground-state $Y(d^1s^2)$ + CH_4 and attractive doublet $Y(d^2s^1)$ + CH_4 surfaces.

In gas-surface-dissociative adsorption, gas phase abstraction reactions (e.g., Cl + CH_4), and in the insertion of a metal atom into a C–H bond, the initial antisymmetric normal mode excitation in the isolated methane molecule is delocalized over four C–H bonds. This energy must evolve into energy localized in the reaction coordinate during approach if reaction is to be successful. Theoretical calculations have allowed us to begin understanding the dynamics of these processes. In the case of dissociative methane adsorption, the symmetric stretch fundamental adiabatically correlates with localized excitation of the unique reacting C–H bond pointing toward the surface (24, 25). However, antisymmetric stretch excitation becomes localized away from the reactive bond in the spectator CH_3 moiety. Qualitatively similar behavior has been observed in theoretical studies of the gaseous abstraction reaction Cl + CH_3D (26).

The subtle complexities underlying the relative efficacy for promoting polyatomic reactions by using different forms of energy are illustrated by the marked differences seen even in closely related systems. For example, Palma *et al.* have carried out theoretical analyses of reactions of ground-state $O(^3P)$ atoms with vibrationally excited CH_4 (27) and CH_3D (28). For CH_4, large enhancement factors were predicted for both symmetric and antisymmetric stretching modes. However, in the deuterium-substituted case, although reactivity was enhanced substantially for symmetric stretching excitation, antisymmetric stretching was not very effective in promoting reaction. Similar subtle effects are evident in the gas–surface systems: translational energy is more effective in promoting reaction of CH_4 than is an equivalent amount of energy in ν_3 for Ni(100), whereas the situation is reversed for Ni(111). Recently, Bisson *et al.* (29) compared the dissociative adsorption of CH_4 ($2\nu_3$) on Pt(111) with that on Ni(111). They found that excitation of CH_4 increases its reactivity by $>10^4$ on Ni(111), whereas the enhancement factor on Pt(111) is $\approx 10^2$. Although a fraction of this difference is attributable to the larger barrier height in the Ni reaction, it has been suggested that, because of a longer C–H bond length at the transition state for Ni than for Pt, reactant vibrational energy is better able to surmount the "later" barrier in the former case.

On the basis of the present results, one might be tempted to conclude by stating that, because the Y + CH_4 insertion reaction is enhanced more strongly by reactant vibrational energy than by an equivalent amount of translational energy, it represents a system involving a "late" potential energy barrier. In a vibrationally nonadiabatic model, reactant vibrational excitation provides access to lower-energy transition state geometries for reaction (7). Although this explanation is appealing, the remarkable subtleties already identified in reactions involving a diverse range of polyatomic systems illustrate that simple concepts based on our understanding of three-atom reactions must be applied with great caution. In the absence of further experiments involving comparisons of other metals and other reactant vibrational modes, and because theoretical analysis remains to be done, generalizations on the basis of our study would be premature. Clearly, the combination of experiment and theory will be of tremendous value in unraveling the fundamental dynamics underlying how different forms of reactant energy promote this important class of chemical reactions.

Experimental Methods

The experimental apparatus employs a laser vaporization source to produce a beam containing ground-state Y atoms in neat H_2 or 20% H_2 in He (30). The beam is collimated by a 2-mm skimmer and a 1.7-mm $\times$ 1.7-mm square defining aperture, refined temporally by using a slotted chopper wheel, and crossed at right angles by singly skimmed beam containing 5% or 10% CH_4 in H_2. For optical pumping experiments, the output of a pulsed narrow-band infrared optical parametric oscillator is arranged to cross the methane beam upstream of the collision region. After bimolecular reaction, some of the chemical products (YCH_2) drift $\approx$25 cm to a detector where they are photoionized by the output of an F_2 laser at 157 nm, pass through a quadrupole mass filter, and are detected by a dynode/electron multiplier combination. The rotatable source assembly makes it possible to rotate the two beams relative to the fixed detector. By measuring the time-of-arrival distributions of the products at the detector, the laboratory angular and kinetic energy distributions are determined for reaction or for nonreactive inelastic collisions.

The OPO is a home-built Nd:YAG pumped unit based on the nonresonant oscillator and optical parametric amplifier stages of a known design (31). The primary differences from that system are the use of a four-crystal (two KTP, two KTA) amplifier stage and the replacement of the SLM OPO with a telecom distributed-feedback diode laser as the seed source (32). The output is spectrally separated in a CaF_2 prism and tuned to the desired absorption resonance by using a photoacoustic cell while measuring the seed wavelength with a fiber-coupled wavemeter. The 3,018 cm^{-1} beam is aligned 5 mm upstream of the interaction region and softly focused to a spot $<$3 mm in diameter in the plane of the beams. The OPO bandwidth has been measured by linewidths in photoacoustic absorption spectra to be $\approx$1 GHz. This is nearly 20 times the expected 41-MHz Doppler width of the ν_3 Q(1) transition transverse to the CH_4 beam calculated from the beam angular divergence; thus, the OPO covers the entire absorption feature. The sharp rise in product signal with the first 100 μJ of IR energy saturation curve in Fig. 5 is consistent with the radiation density provided by the OPO and the known oscillator strength of the transition. The much slower increase in signal at higher energies is characteristic of a beam profile containing a distribution of intensities and the trendline in Fig. 5 has been calculated by using such a distribution. This is consistent with the nonuniform beam profile observed with this OPO and typical of this design.

Determination of the fraction of the CH_4 beam pumped by the OPO is as follows. The hydrogen nuclear spin statistics in methane are such that each of the nuclear modifications has a different lowest allowed J state: J = 0, 2, and 1 for the A, E, and F modifications, respectively (33). Modifications do not exchange on the microsecond time scale of a supersonic expansion, so in the limit of complete rotational cooling the populations of each of these J states in the beam are identically the populations of the modifications at room-temperature thermal equilibrium: 5/16, 2/16, and 9/16 for A (J = 0), E (J = 2), and F (J = 1) respectively (34). We pumped the Q(1) line of ν_3, so the lower state is J = 1 and the maximum fractional population is 9/16. The OPO saturated the transition, so the excitation fraction is given by the ratio of the upper-state statistical weight to the sum of the upper- and lower-state statistical weights (35). Both states have an extra threefold degeneracy from the F modification in addition the normal ($2J$ + 1) rotational degeneracy for a total of nine, as tabulated in the HITRAN database (36). The saturated fractional excitation is thus 1/2. The fraction of the gas pulse that was illuminated was calculated geometrically. The Y beam was mechanically chopped by a slotted disk of 10.9-cm radius with a 1-mm-wide slit spinning at 210 Hz providing a shutter function that is $\approx$7.0 μs wide. The methane (10% in H_2) beam has a mean velocity of 2,123 m/s, so a 7.0-μs pulse is 14.9 mm long. The 3.0-mm spot size of the OPO in the plane of the beams thus illuminates 20% of the beam. The fraction of the methane flux in the ν_3 state is therefore (9/16)(1/2)(0.20) = 5.6%.

ACKNOWLEDGMENTS. This work was supported by the National Science Foundation Grant CHE-0316296.

1. Polanyi JC (1987) Some concepts in reaction dynamics. *Science* 236:680–690.
2. Crim FF (1999) Vibrational state control of bimolecular reactions: Discovering and directing the chemistry. *Acc Chem Res* 32:877–884.
3. Zare RN (1998) Laser control of chemical reactions. *Science* 279:1875–1879.
4. Yan S, Wu Y-T, Zhang B, Yue X-F, Liu K (2007) Do vibrational excitations of CHD_3 preferentially promote reactivity toward the chlorine atom? *Science* 316:1723–1726.
5. Crim FF (2007) Making energy count. *Science* 316:1707–1708.
6. Juurlink LBF, McCabe PR, Smith RR, DiCologero CL, Utz AL (1999) Eigenstate-resolved studied of gas-surface reactivity: CH_4 (i_3) dissociation on Ni(100). *Phys Rev Lett* 83:868–871.
7. Smith RR, Killelea DR, DelSesto DF, Utz AL (2004) Preference for vibrational over translational energy in a gas-surface reaction. *Science* 304:992–995.

8. Higgins J, Conjusteau A, Scoles G, Bernasek SL (2001) State selective vibrational ($2i_3$) activation of the chemisorption of methane on Pt(111). *J Chem Phys* 114:5277–5283.
9. Juurlink LBF, Smith RR, Killelea DR, Utz AL (2005) Comparative study of C-H stretch and bend vibrations in methane activation on Ni(100) and Ni(111). *Phys Rev Lett* 94:208303.
10. Maroni P, *et al.* (2005) State resolved gas-surface reactivity of methane in the symmetric C-H stretch vibration on Ni(100). *Phys Rev Lett* 94:246104.
11. Lersch M, Tilset M (2005) Mechanistic aspects of C-H activation by Pt complexes. *Chem Rev* 105:2471–2526.
12. Godula K, Sames D (2006) C-H bond functionalization in complex organic synthesis. *Science* 312:67–72.
13. Niu S, Hall MB (2000) Theoretical studies of reactions of transition-metal complexes. *Chem Rev* 100:353–405.
14. Wittborn AMC, Costas M, Blomberg MRA, Siegbahn PEM (1997) The C-H activation reaction of methane for all transition metal atoms from the first three rows. *J Chem Phys* 107:4318–4328.
15. Carroll JJ, *et al.* (1995) Gas phase reactions of second-row transition metal atoms with small hydrocarbons: Experiment and theory. *J Phys Chem* 99:13955–13969.
16. Henkelman G, Jonsson H (2001) Theoretical calculations of dissociative adsorption of CH_4 on an Ir(111) surface. *Phys Rev Lett* 86:664.
17. Nave S, Jackson B (2007) Methane dissociation on Ni(111): The role of lattice reconstruction. *Phys Rev Lett* 98:173003.
18. Stauffer HU, Hinrichs RZ, Schroden JJ, Davis HF (2000) Dynamics of H_2 and C_2H_4 production from Y + C_2H_6 reactions. *J Phys Chem A* 104:1107–1116.
19. Li T, Cheng W, Liu J, Xie X, Cao H (2006) A computational study on the reaction of yttrium with ketene. *J Mol Struct Theochem* 761:83–88.
20. Blomberg MRA, Siegbahn PEM, Svensson M (1992) Mechanisms for the reactions between methane and the neutral transition metal atoms from yttrium to palladium. *J Am Chem Soc* 114:6095–6102.
21. Lee YT (1988) *Atomic and Molecular Beam Methods*, ed Scoles G (Oxford Univ Press, New York), Vol I, pp 553–568.
22. Bronnikov DK, *et al.* (1998) Spectroscopy and non-equilibrium distribution of vibrationally excited methane in a supersonic jet. *J Quant Spectrosc Radiat Transfer* 60:1053–1068.
23. Willis PA, Stauffer HU Hinrichs RZ, Davis HF (1999) Reaction dynamics of Zr and Nb with ethylene. *J Phys Chem A* 103:3706–3720.
24. Halonen L, Bernasek SL, Nesbitt DJ (2001) Reactivity of vibrationally excited methane on nickel surfaces. *J Chem Phys* 115:5611–5619.
25. Milot R, Jansen APJ (2000) Bond breaking in vibrationally excited methane on transition-metal catalysts. *Phys Rev B* 61:15657–15660.
26. Yoon S, Holiday RJ, Sibert EL III, Crim FF (2003) The relative reactivity of CH_3D molecules with excited symmetric and antisymmetric stretching vibrations. *J Chem Phys* 119:9568–9575.
27. Palma P, Clary DC (2000) The effect of the symmetric and asymmetric stretching vibrations on the $CH_4 + O(^3P) \rightarrow OH + CH_3$ reaction. *Phys Chem Chem Phys* 2:4105–4114.
28. Palma P, Echave J, Clary DC (2002) The effect of the symmetric and asymmetric stretching vibrations on the $CH_3D + O(^3P) \rightarrow CH_3 + OD$ reaction. *Chem Phys Lett* 363:529–533.
29. Bisson R, *et al.* (2007) State-resolved reactivity of CH_4 ($2\nu_3$) on Pt(111) and Ni(111): Effects of barrier height and transition state location. *J Phys Chem A* 111:12679–12683.
30. Willis PA, Stauffer HU, Hinrichs RZ, Davis HF (1999) Rotatable source crossed molecular beams apparatus with pulsed VUV photoionization detection. *Rev Sci Instrum* 70:2606–2614.
31. Bosenberg WR, Guyer DR (1993) Broadly tunable, single-frequency optical parametric frequency-conversion system. *J Opt Soc Am B* 10:1716–1722.
32. Kulatilaka WD, Anderson TN, Bougher TL, Lucht RP (2005) Development of injection–seeded, pulsed optical parametric generator/oscillator systems for high-resolution spectroscopy. *Appl Phys B* 80:669–680.
33. Herzberg G (1945) *Molecular Spectra and Molecular Structure II. Infrared and Raman Spectra of Polyatomic Molecules* (D. Van Nostrand, Princeton, NJ), pp 37–42.
34. Hepp M, Winnewisser G, Yamada KMT (1994) Conservation of the nuclear spin modification of CH_4 in the cooling process by supersonic jet expansion. *J Mol Spec* 164:311–314.
35. Bernstein RB (1982) *Chemical Dynamics via Molecular Beam and Laser Techniques* (Oxford Univ Press, New York), pp 38–44.
36. Rothman LS, *et al.* (2005) The HITRAN 2004 molecular spectroscopic database. *J Quant Spec Rad Trans* 96:139–204.